Analysis of the Effects of Atmospheric Noise on LORAN-C

Curtis Cutright, Jonathon Sayre, Frank van Graas
Avionics Engineering Center, Ohio University

ABSTRACT

The Federal Aviation Administration is currently funding research to determine the feasibility of using LORAN for enroute and non-precision approach guidance as a backup to the Global Positioning System (GPS). The signal-to-noise ratio (SNR) of the received LORAN-C signal is one of the key factors in determining the usefulness of LORAN-C signals for navigation. The effects of atmospheric noise, such as precipitation static and thunderstorms, can have a significant impact on the SNR of LORAN signals. Ohio University's Avionics Engineering Center (AEC) has been conducting flight tests for the past year to collect data in the presence of these atmospheric noise conditions. This data will allow the effects of the atmospheric noise on the LORAN SNR to be characterized. Accurately characterizing these effects will play a major role in the accuracy, integrity, availability, and continuity analysis of the LORAN system.

Flight tests have been conducted at several locations under varying weather conditions. LORAN data was collected using a two-channel data collection device to simultaneously collect radio frequency (RF) data from two independent antennas. Both e-field and h-field antennas are used to allow for comparison of the data so analysis of the performance of each antenna in varying environments can be accomplished. An identical data collection system is used to simultaneously collect ground data to be used as a baseline reference.

Characterizing the effect of aircraft charging and discharging is also important in studying the effects of noise on the LORAN signal. The charge built up on the aircraft during flight through inclement weather and the way that charge is dissipated by the aircraft introduces noise into the LORAN spectrum. In order to study these effects, the static dischargers on the Douglas DC-3 used during the flight testing conducted at the Kendall-Tamiami Executive Airport during July 2005 were instrumented. This allowed the charge being dissipated by the static wicks during flight to be measured and recorded. In addition, a field mill was installed on the aircraft to record the level of the static charge on the aircraft to be recorded.

This paper will describe the data collection system used by AEC. Examples of the data collected by both the in-flight and ground-based systems will be presented. Results of the data analysis and comparisons between the ground and airborne data will be presented.

1. INTRODUCTION

The Long Range Navigation (LORAN) system has been in use since World War II as a position, navigation, and timing system. However, LORAN-C has typically had fairly large (100-500 meter) errors in its position solution performance. In addition, its use as an airborne navigation system has been hampered by problems caused by climatic effects (changes in propagation path), aircraft induced effects (precipitation static), and atmospheric effects (lightning).

The introduction of new navigation systems has gradually reduced the use of LORAN-C as a primary means for point-to-point navigation, especially for aviation. Most notably, the Global Positioning System (GPS) has provided the capability for worldwide navigation using a single system. However, the results of recent studies, such as the Volpe Report cited in reference 1, have shown a change in thinking when considering the use of GPS as the sole source of positioning in the National Airspace System (NAS).

The LORAN Integrity and Performance Panel (LORIPP) was one of two panels formed by the Federal Aviation Administration (FAA) LORAN-C Program Office to evaluate the use of LORAN as a backup navigation system. The panels were formed to bring together individuals capable of determining the changes that would be required to allow LORAN to serve as a suitable backup to GPS. These changes will allow the new enhanced LORAN (eLORAN) system to meet the Required Navigation Performance (RNP) for non-precision approach (NPA) procedures.

As part of this panel, the Avionics Engineering Center (AEC) at Ohio University was tasked to evaluate the effects of atmospheric noise and precipitation static (p-static) on LORAN-C navigation performance. Collecting data that would allow these weather-related effects to be observed required that a data collection system capable of capturing radio frequency (RF) signals in the LORAN-C frequency band be fielded. The results obtained from the data collected using this system have been shown in previous papers [1] [2].

However, it has been determined from those results that additional information will be required to adequately identify the atmospheric processes that cause problems for the LORAN system. The additional data will allow for better analysis of the mechanisms involved which cause atmospheric interference with the LORAN signal. As a first step, AEC has added to its data collection system the capability to record aircraft static-wick discharge currents and aircraft charging voltage.

This paper will provide an overview of the new aircraft data collection system. The methods used to calibrate the aircraft charging data collection equipment and the results of the calibration testing will be presented. Also, an initial report on AEC's first data collection mission using the new system, conducted in July of 2005 at the Kendall-Tamiami Executive Airport in Miami, FL, will be provided.

2. Data Collection System

2.1. Overview

The primary goal of the LORAN data collection system designed at Ohio University is to collect RF data in the LORAN frequency band. The system was designed so that the data being collected provide an accurate representation of the data that would be seen by a typical LORAN receiver.

Data is collected during flight testing using both airborne and ground-based data collection systems. The ground data is used as a baseline for the airborne data to help identify sources of interference that are not the result of atmospheric noise. The equipment that has been added to the airborne system is designed to collect data from instrumented static wicks installed on the aircraft wings and tail and a field mill installed on the belly of the aircraft.

2.2. Airborne System

Figure 1 shows the data collection system installed on AEC's Douglas DC-3, shown in Figure 2.

The data collection PC and the chassis containing the data collection equipment are mounted in a 19-inch rack; the rack is installed on the seat rails of the aircraft. Unlike the King Air C-90SE on which the equipment has previously been installed, the DC-3 does not have a storm scope that provides the capability to record lightning-strike activity. Both e-field and h-field antennas are used in the data collection system. They are of the same type as the antennas used in the King Air setup; however, the e-field antenna used during the DC-3 flight testing was the ship's antenna.

Figure 1: Data collection equipment rack

The data collection box contains the Reelektronika DataGrabber, which is used to collect LORAN-C RF data, and a GPS receiver from which position data is collected during flight.

Figure 2: Ohio University's Douglas DC-3

A description of the airborne RF data collection system equipment is contained in reference 2.

The new data collection system consists of the previously fielded RF data collection system and the equipment being used to collect the aircraft charging data. This equipment includes a field mill, instrumented static wicks, and a data collection system chassis. The front panel of the new data collection system chassis is shown in Figure 3.

Figure 3: Charging Data Collection System Chassis

Figure 4 shows the internal components of the chassis.

Figure 4: Charging Data Collection System Chassis Internal Components

The chassis contains the control head for the field mill and the instrumentation required to collect the aircraft charging data and transmit it to the data collection PC for recording.

The field mill used in the new data collection system setup is shown in Figure 5. It is used to measure the electrostatic field strength surrounding the aircraft. Since there is no ground plane under the field mill while the aircraft is in-flight all the measurements are relative to the charge on the aircraft. The field mill chosen was a Mission Instruments EFS-1001 Electrostatic Field Mill. This field mill was chosen primarily because it was the model used by the Federal Aviation Administration Technical Center (FAATC) in their equipment setup on their Aero Commander, detailed in reference 3. At some point in time, this will facilitate easier data comparison between the two group's results.

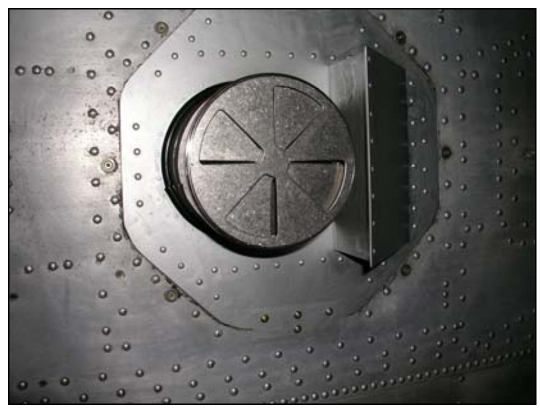

Figure 5: EFS-1001 Field Mill

The field mill has a range of ±100kV. The output of the field mill is sent to a digital voltmeter that is part of the aircraft charging data collection system. The module used is a DGH Corporation Model D1142 Voltage Input Module. The Model D1142 has an input voltage range of ±10V. The output of the field mill is scaled so that the full-scale deflection of the field mill causes a corresponding full-scale deflection of the D1142 voltage input module. The module converts the analog input to a digital output which is sent out over a serial connection to the data collection PC.

Aircraft static-wick discharge current data are collected from the five aircraft static wicks which have been instrumented.

These five static wicks are: left wing (LW), right wing (RW), left elevator (LE), right elevator (RE), and the rudder (RU).

An example of an instrumented static wick is shown in Figure 6. The static wicks are isolated from the discharger bases using a non-conductive barrel. A shielded wire is then run from the wick to the new data collection system chassis which contains the data collection modules. The shields of the wires from the static wicks are terminated on one end to help prevent noise from the aircraft systems or other sources from affecting the current measurements.

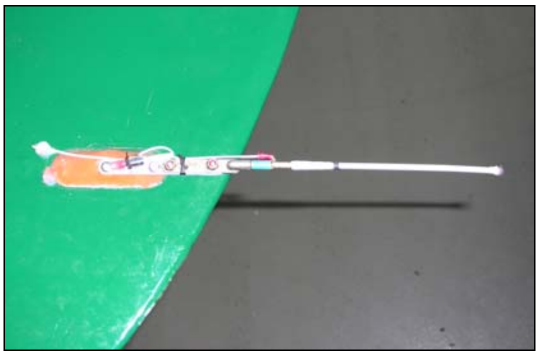

Figure 6: Instrumented Static Wick

Current data is collected using five DGH Model D1222 Current Input Modules. Like the module used for the field mill, these convert the analog current measurements to digital and transmit them to the data collection PC over a serial communication line. The D1222 modules have a range of ±1mA.

2.3 Ground System

Figure 7 shows the ground data collection system van used to collect data at the Kendall-Tamiami Executive Airport in Florida.

The ground data collection system uses the same LORAN-C equipment as used in the airborne system. This provides the capability to collect baseline data during flight testing for comparison with the airborne data. A more detailed description of the ground data collection system can be found in reference 4.

Figure 7: Ground Data Collection System

3. Equipment Calibration

3.1 Overview

The aircraft charging data collection equipment was calibrated to determine how accurately it was recording aircraft discharge currents and aircraft electrostatic charge buildup. Several tests were performed to ensure repeatability of the results. In addition, the field mill was calibrated separately to accurately characterize its performance. This section will describe the equipment used to perform the tests, outline the methods used for the field mill and total system testing, and show the results of the calibration tests.

3.2 Calibration Equipment

High-voltage test equipment capable of charging the DC-3 to known levels was used for the calibration testing. This equipment allows charging levels to be controlled to ensure the safety of the aircraft and the personnel performing the testing. Aircraft discharge currents are also recorded to ensure that all current being transferred to the aircraft is accounted for as it is discharged from the aircraft.

The high voltage test equipment includes: a high voltage power supply, flood fixtures to transfer the charge to the aircraft, collectors to remove the charge from the aircraft, and a ground data collection system to record the data.

The high voltage power supply is shown in Figure 8. The supply will output up to 50kV. The output voltage is controlled using a single phase variable AC power transformer.

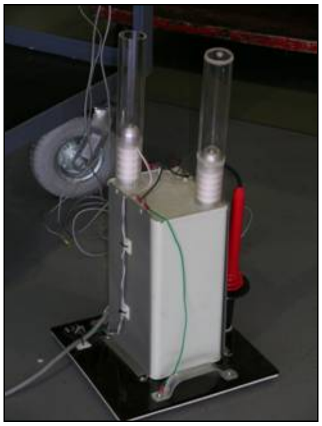

Figure 8: High Voltage Power Supply

Flood fixtures are used to distribute the charge from the power supply to the aircraft. A typical flood fixture setup is shown in Figure 9. The flood fixtures are connected to the power supply using ignition wire capable of handling the high voltage being generated by the power supply.

Figure 9: Typical Flood Fixture Setup

Collector fixtures are placed behind the aircraft static discharge wicks to draw the current off the aircraft. The left elevator collector is shown in Figure 10.

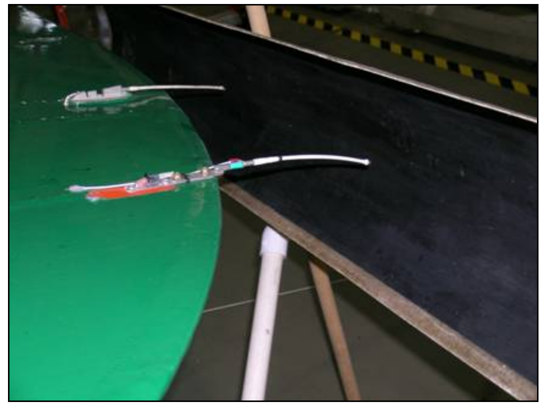

Figure 10: Collector Fixture

Wires are run from each collector to the data collection system shown in Figure 11. This allows the total current being drawn from the aircraft to be monitored. These currents are summed by the equipment so that the total current being removed from the aircraft can be compared to the high voltage power supply current. This provides a means to detect current that is not being drawn off through the aircraft static dischargers which could lead to inaccurate discharger calibration.

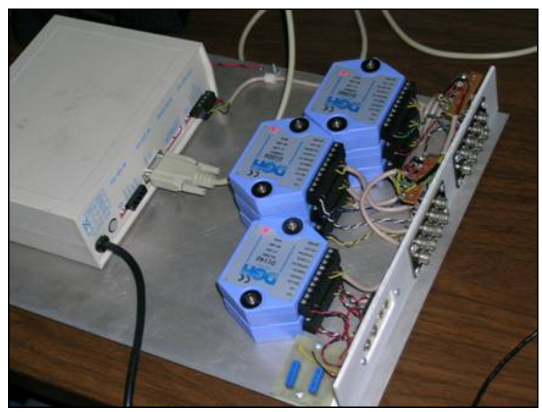

Figure 11: Ground Data Collection System

The ground data collection system uses the same DGH modules that are used in the aircraft system. A panel of LED displays is also used to allow the equipment operator to monitor the test in real-time. The data is collected using a laptop computer.

3.3 Field Mill Calibration

The field mill calibration was performed using the calibration fixture shown in Figure 12. The fixture was built by AEC and is designed to allow a known charge to be applied across two uniformly spaced plates.

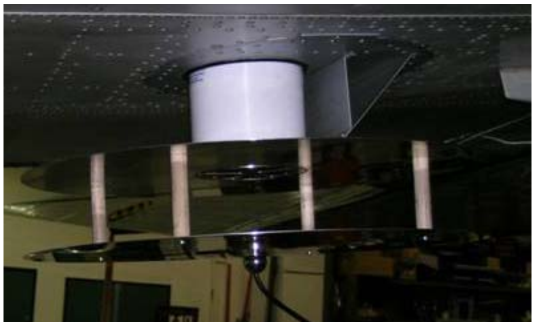

Figure 12: Field Mill Calibration Fixture

The fixture consists of two metal plates placed 10cm apart. The plates are joined using non-conductive wooden dowel rods. The high voltage power supply is connected to the lower plate and the upper plate is connected to a common ground used for the power supply to create a ground reference plane. This creates a field of a known strength that can be measured by the field mill.

The results of the field mill calibration are shown in Figure 13. Since the voltages are applied across a 10cm plate, the field mill results have been scaled by a factor of ten to allow for comparison to the power supply data.

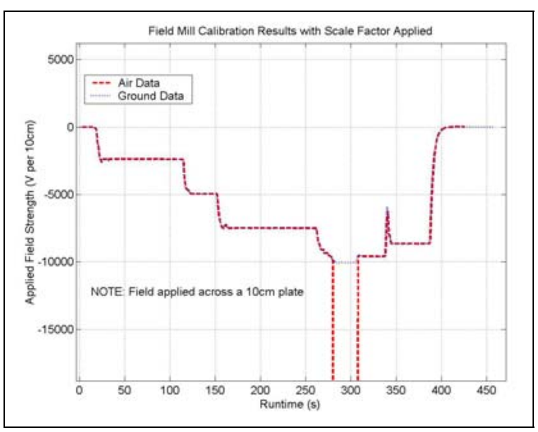

Figure 13: Field Mill Calibration Results

The results show that the field mill is accurately recording the field being applied to the calibration fixture. When the voltage applied to the calibration fixture exceeded the range of the field mill the measurements indicate an out-of-range condition which is represented by an output value from the DGH module of -100kV.

3.4 System Calibration

The goal of the system calibration is to accurately characterize the aircraft charging data collection system with the aircraft in a configuration as close as possible to the in-flight conditions. However, the calibration procedure does have limitations. Since the charge is applied to the aircraft and removed from the aircraft in specific locations, effects from spurious discharges that may occur in-flight around other locations may not be observed. It is reasonable, though, to assume that most of the charge is dissipated from these locations since the aircraft is designed and certified to fly with only the static dischargers for protection against charge buildup.

The results from one of the calibration runs are shown below. Figure 14 shows the field mill readings from the aircraft versus the voltage being applied from the power supply. The field mill measurements are made with reference to a plate placed approximately 1.15m below the field mill. This plate is connected to the same ground that is used by the high voltage power supply. This ensures that the aircraft is not recording different voltage levels due to a difference in the reference ground plane.

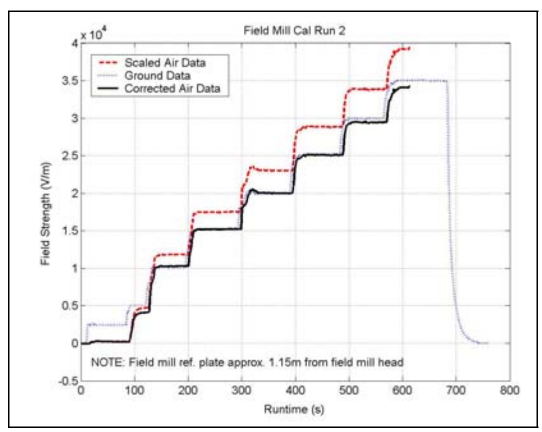

Figure 14: System Calibration - Field Mill

The aircraft readings were corrected to account for the 1.15m distance between the field mill and the reference plate. They show good agreement with the voltage being applied to the aircraft. The slight difference in the measurements is attributed to the fact that the aircraft does not always uniformly distribute the charge being applied. In-flight, these differences can be even greater with variations of tens of kilovolts between areas of the aircraft skin.

The results from the left wing static discharger are shown in Figure 15. The red dashed line is the aircraft data and the ground data is plotted with the blue dashed line. Although the total current being measured by the aircraft and ground show significant differences, the trends in both data sets are in good agreement. The differences in the currents being measured are due to the fact that while multiple dischargers are being effectively recorded through the collection fixture, only the outboard discharger current is being recorded by the aircraft.

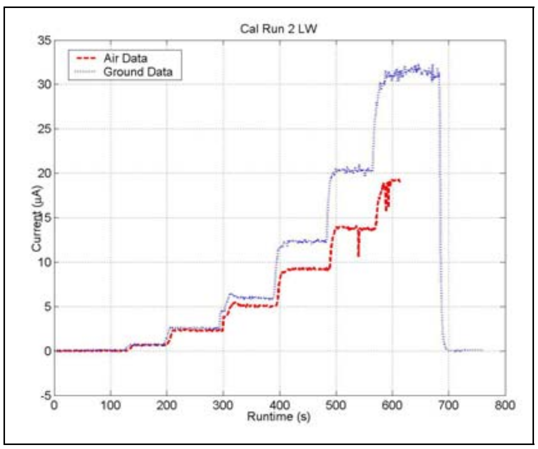

Figure 15: System Calibration - Left Wing

The results for the other dischargers were similar and appear in Appendix A.

3.5 Discharger Test

The last test conducted during the calibration was to confirm that all the current being discharged from the aircraft was dissipated through the aircraft static wicks. This was accomplished by removing all but the instrumented static dischargers from the aircraft. This forced all the charge being removed by the collector fixtures to be carried by the remaining instrumented wick.

The results of this test for the left wing discharger are shown in Figure 16. The plot shows that with the non-instrumented dischargers removed all the charge being recorded by the ground data collection system for the left wing is being carried through the remaining discharger.

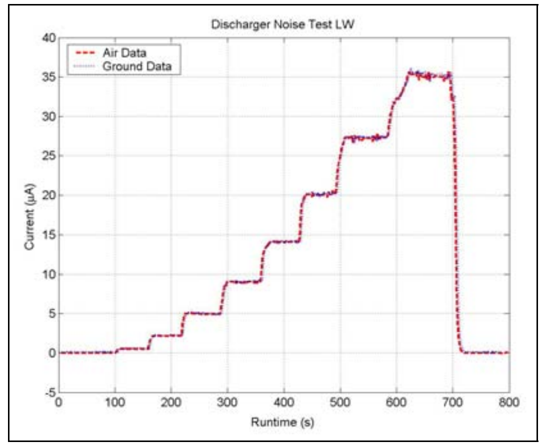

Figure 16: Discharger Test - Left Wing

Since the individual collector fixture currents added up to the total current being output by the power supply, this ensures that no current is being discharged through other parts of the aircraft during these tests. The results for the other four instrumented dischargers and the field mill appear in Appendix B. All dischargers showed behavior similar to the left wing.

4. Flight Test Overview

4.1 Location

Flight tests were conducted in southern Florida from July 5-15, 2004. As with previous flight testing accomplished last year using AEC's King Air C-90B, the Kendall-Tamiami Executive Airport (TMB) was again used as the staging location for these flight tests. This allowed for better comparison between the data, both air and ground, that was previously collected.

4.2 Equipment Setup

The ground data collection van, shown in Figure 7, was positioned near the glideslope shelter which is part of the National ILS Test Facility run by AEC. This is the location that was chosen last year due to ready availability of ground power and lack of overhead power lines or large buildings in the surrounding area. In addition, this location allowed the DC-3 to be parked within 200 yards of the van so baseline data could be collected on both systems under similar conditions.

Data were collected in the van using the ground data collection system during all the flight tests. Only battery power was used to run the equipment as it has been determined from previous testing that commercial power introduces additional noise into the data.

4.3 Description

Two flight tests totaling approximately five hours were flown during which significant atmospheric activity was encountered. The flight conducted on July 12th lasted approximately 3.5 hours during which several areas of p-static were found. The July 13th flight test consisted mainly of circling overhead the airport for approximately one hour. Several lines of thunderstorms were moving through the area at the time and they provided the opportunity to collect data close to the ground data collection site.

Ground data were collected during all the flight testing. Results from the ground data collection are not shown in this paper. The presence of several additional noise sources not apparent during previous testing will require additional data processing to yield useful results. Once completed, this data will be used as a baseline for the airborne data collected, most significantly for the data collected near TMB during a flight conducted with moderate thunderstorms in the vicinity of the airport.

5. Results

5.1 Overview

A period of data from each of the flights was chosen to be processed. The data sets are representative of the periods of the most severe p-static and lightning activity found during the flight.

The data was processed using the methods previously detailed in reference 3; a histogram of the noise is generated from the results of the processing. The flight path flown during the test is also shown for each of the data sets. Plots are included to illustrate the effect of the noise on the RF signal. The ability of the data processing software to isolate and remove LORAN pulses and the measurements from the aircraft charging data collection equipment are also shown.

5.2 July 12, 2005 Flight Test Results

The results shown here are from data that was collected during this flight test while flying through a region of severe p-static activity. The flight path is shown in Figure 17. The area in black shows where this data was collected during the flight.

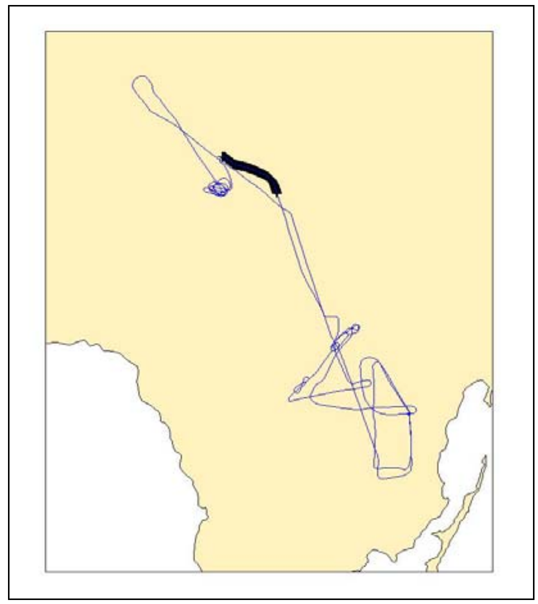

Figure 17: July 12 Flight Path

A two-second sample of the RF data collected during this period is shown in Figure 18.

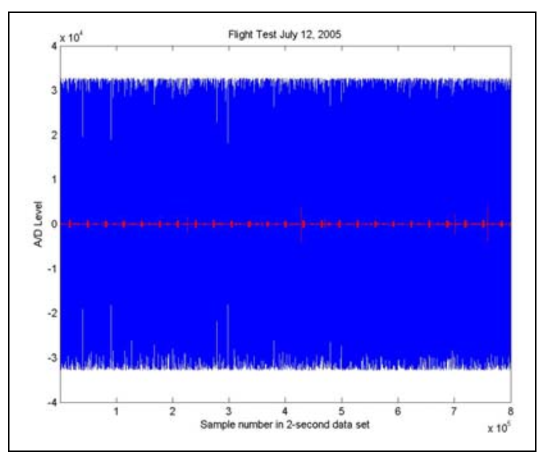

Figure 18: July 12 RF Data

The plot shows that during this period, the e-field signal appears to have been lost in the p-static noise which is exceeding the maximum range of the A/D converter in the DataGrabber. In the plot, the e-field signal is blue and the h-field signal is red and can be seen silhouetted against the e-field LORAN pulses.

The h-field signal appears to be unaffected, as can be seen in the zoomed-in view shown in Figure 19.

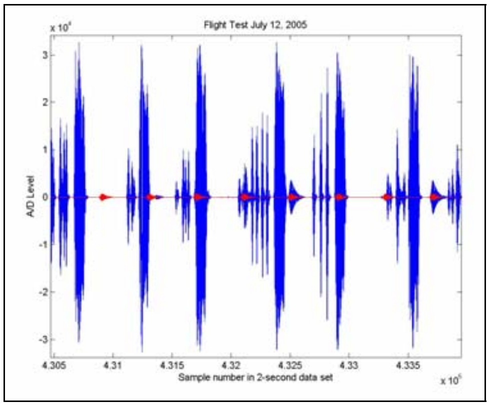

Figure 19: July 12 RF Data (Zoomed)

Appendix C contains the plots of the results for this data set. The tracking results show that for much of the data set the e-field signal could not be tracked by the data processing software. The h-field signal is tracked through the data set without interruption. The noise histograms indicate agreement with the tracking data. The e-field results clearly show that the noise pulses seen by the e-field antenna are at much higher levels than the h-field antenna. The h-field histogram shows the Gaussian distribution that would be expected from atmospheric noise.

The charging results data show that during this period the aircraft charged and discharged. As the aircraft discharged the data recorded from the static wicks showed a corresponding increase in current flow. The field mill recorded maximum field strength of over 65kV/m during this time.

5.3 July 13, 2005 Flight Test Results

The ground track from the July 13th flight test is shown in Figure 20. The results shown are from data collected in the area highlighted in black; this is shown more clearly in Figure 21. A holding pattern was established over the airport and orbits were flown for approximately one hour.

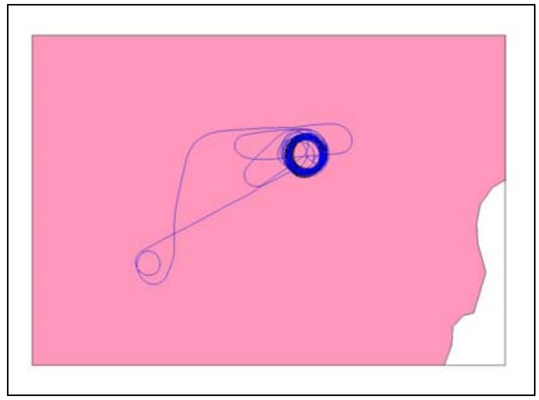

Figure 20: July 13 Flight Path

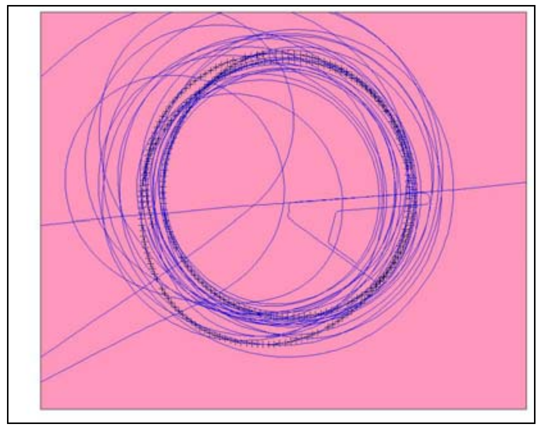

Figure 21: July 13 Flight Path (Zoomed)

A sample of the RF data is shown in Figure 22. This 2-second data sample shows the noise caused by the lightning strikes from the nearby thunderstorm cells. These strikes occur throughout the data set with varying frequency and power.

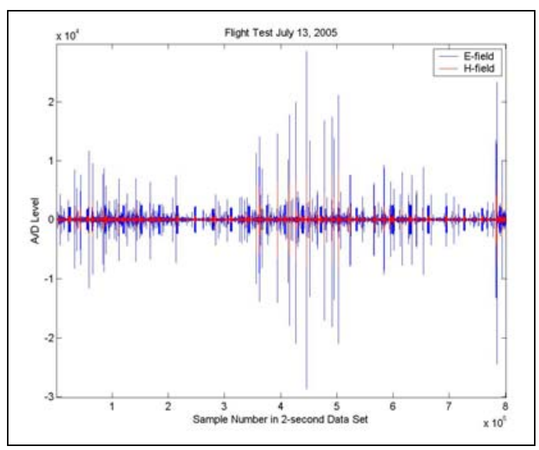

Figure 22: July 13 RF Data

However, the close-up detail in Figure 23 shows that LORAN pulses are still visible in the data. As expected, this view also shows that unlike the data collected during the periods of p-static, the lightning strikes appear to affect both the e-field and h-field signals in a similar manner.

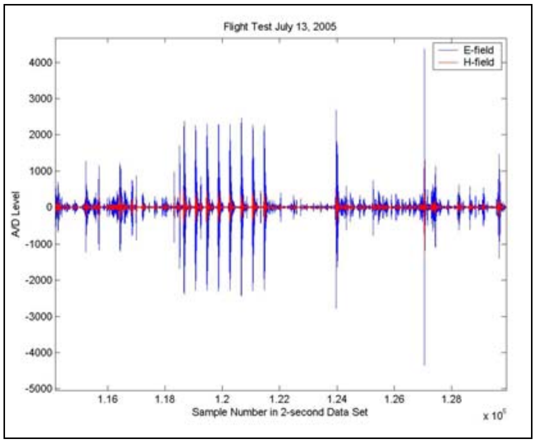

Figure 23: July 13 RF Data (Zoomed)

The remaining results are contained in Appendix D. They show that both the e-field and h-field signals were tracked continuously throughout the five-minute data set chosen. The histograms of the RF data indicate that both antennas were affected in similar ways. Both of these plots show that the noise, even in the presence of the lightning strikes, appears Gaussian in nature and the e-field data lacks the large tails seen in the data set containing p-static.

6. Conclusions

The charging data show that the lightning strikes had very little, if any, effect on the aircraft. Further data analysis may show that the results seen during this period are almost completely due to normal aircraft charging that occurs even during flight through areas with no significant weather activity.

These preliminary results indicate that the primary source of atmospheric interference for LORAN is caused by p-static. The data also show that even this effect is almost entirely mitigated by the use of an h-field antenna.

These results indicate that with the use of a properly designed h-field antenna and the advanced data-processing techniques made possible by the increased computational power available today, versus when the LORAN system was designed, the effects of atmospheric noise should not pose a serious threat to the ability to navigate using an eLORAN system.

7. Future Work

The remaining data needs to be processed to determine if the results seen in the initial data analysis are found throughout all of the data sets. This data will then need to be compared to previously collected data to allow for a more complete analysis that encompasses varying levels of both p-static and lightning activity.

In addition, work will need to be done to develop a system capable of more accurately recording the lightning activity being experienced so a more thorough characterization of the lightning being experienced during the flight tests can be made. This will allow for a more accurate assessment of the effects of lightning based on strike amplitude, distance, and location.

The possibility of using modified e-field antennas should also be investigated. If the capability to design an e-field antenna that is less susceptible to p-static effects can be developed, many known issues that arise from the use of h-field antennas can be avoided.

Acknowledgements

This work was performed under Federal Aviation Administration contract DTFA01-01-C-0071 Technical Task Directive 2.1 – LORAN-C Analysis and Support. The authors would like to thank the Program Office Manager, Mr. Mitchell J. Narins, for his assistance in making this research possible. In addition, thanks are due to Dr. Richard McFarland and Bryan Branham, our DC-3 pilots, and Mr. Michael Handrahan, Kendall-Tamiami Executive Airport manager. The help of Dave Diggle, Dave Quinet and Frank van Graas at AEC has also been invaluable throughout this project.

References

[1] John A. Volpe National Transportation Systems Center, "Vulnerability Assessment of the Transportation Infrastructure Relying on the Global Positioning System", August 29, 2001

[2] Cutright, C., et al., “LORAN-C Band Data Collection Efforts at Ohio University”, Proceedings of the International LORAN Association (ILA-32) Convention and Technical Symposium, Boulder, Colorado, November 3-7, 2003

[3] Lilley, R., R. Erikson, “FAA Tests E- and H-Field Antennas to Characterize Improved LORAN-C Availability During P-Static Events”, Proceedings of the International LORAN Association (ILA-33) Convention and Technical Symposium, Tokyo, Japan, October 25-27, 2004

[4] Cutright, C., et al., “Analysis of the Effects of Atmospheric Noise on LORAN-C”, Proceedings of the International LORAN Association (ILA-33) Convention and Technical Symposium, Tokyo, Japan, October 25-27, 2004

Appendix A

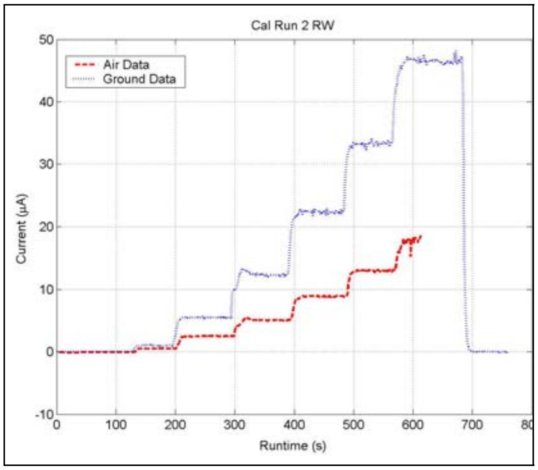

Figure A1: Right Wing

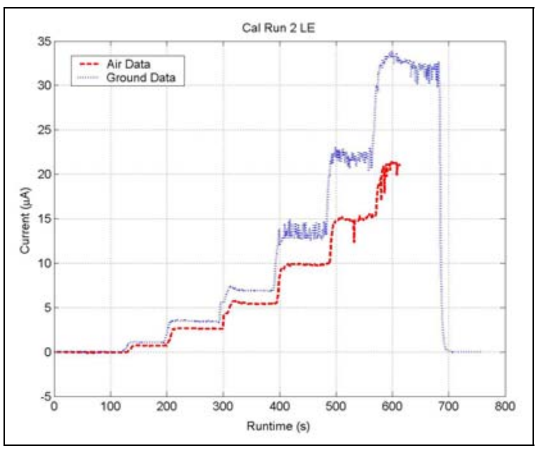

Figure A2: Left Elevator

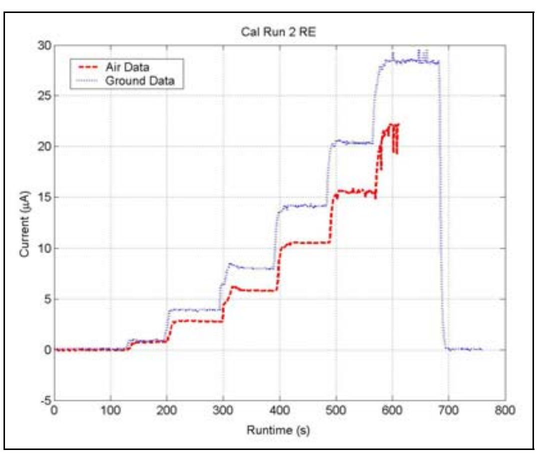

Figure A3: Right Elevator

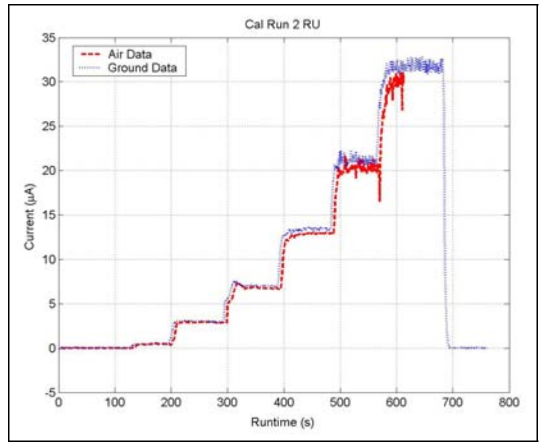

Figure A4: Rudder

Appendix B

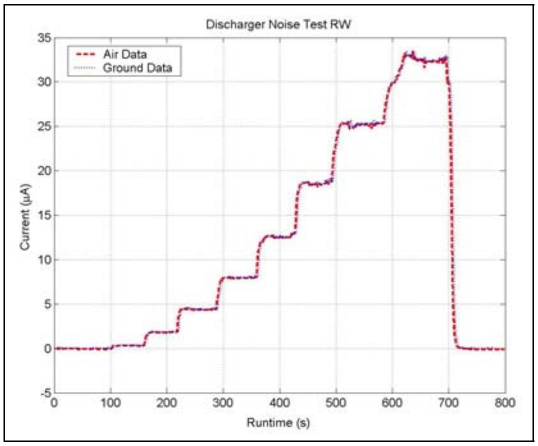

Figure B1: Right Wing

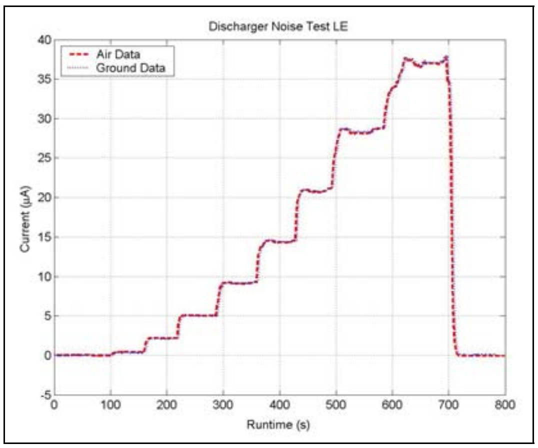

Figure B2: Left Elevator

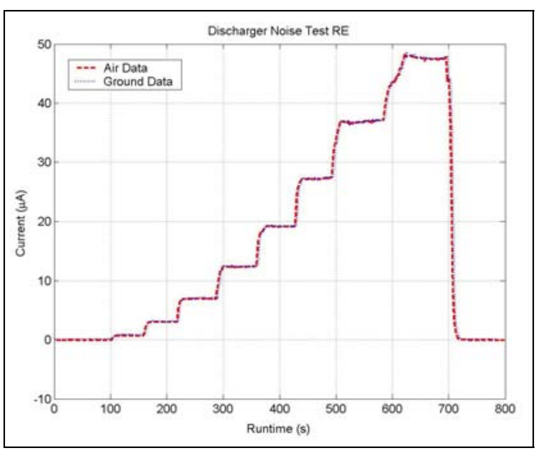

Figure B3: Right Elevator

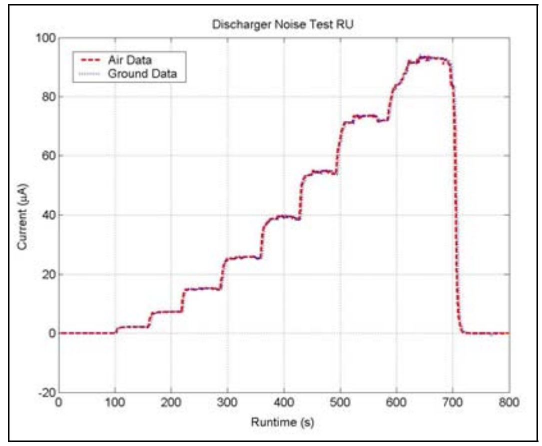

Figure B4: Rudder

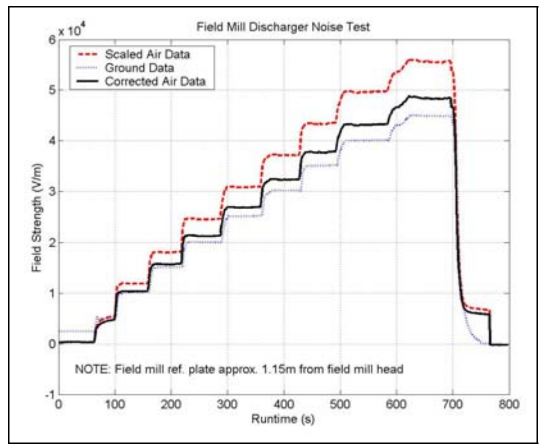

Figure B5: Field Mill

Appendix C

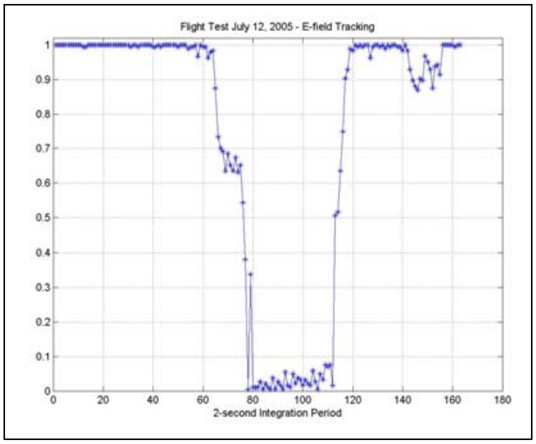

Figure C1: E-field Tracking Results

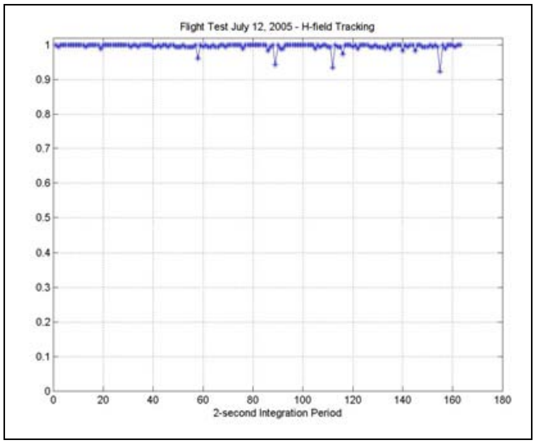

Figure C2: H-field Tracking Results

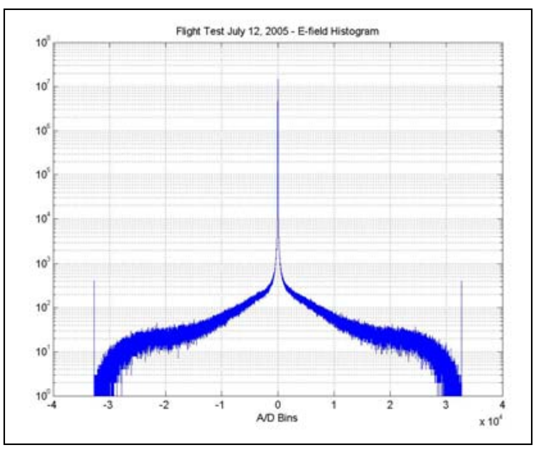

Figure C3: E-field Histogram

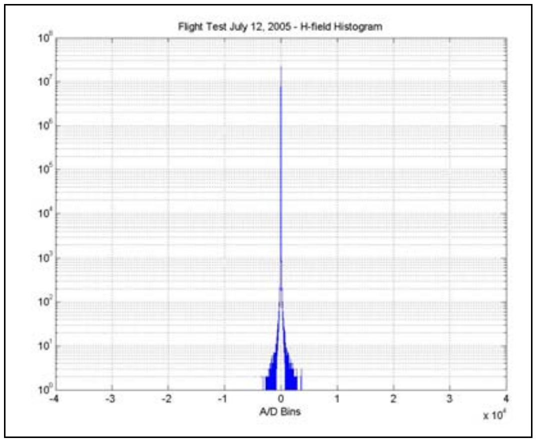

Figure C4: H-field Histogram

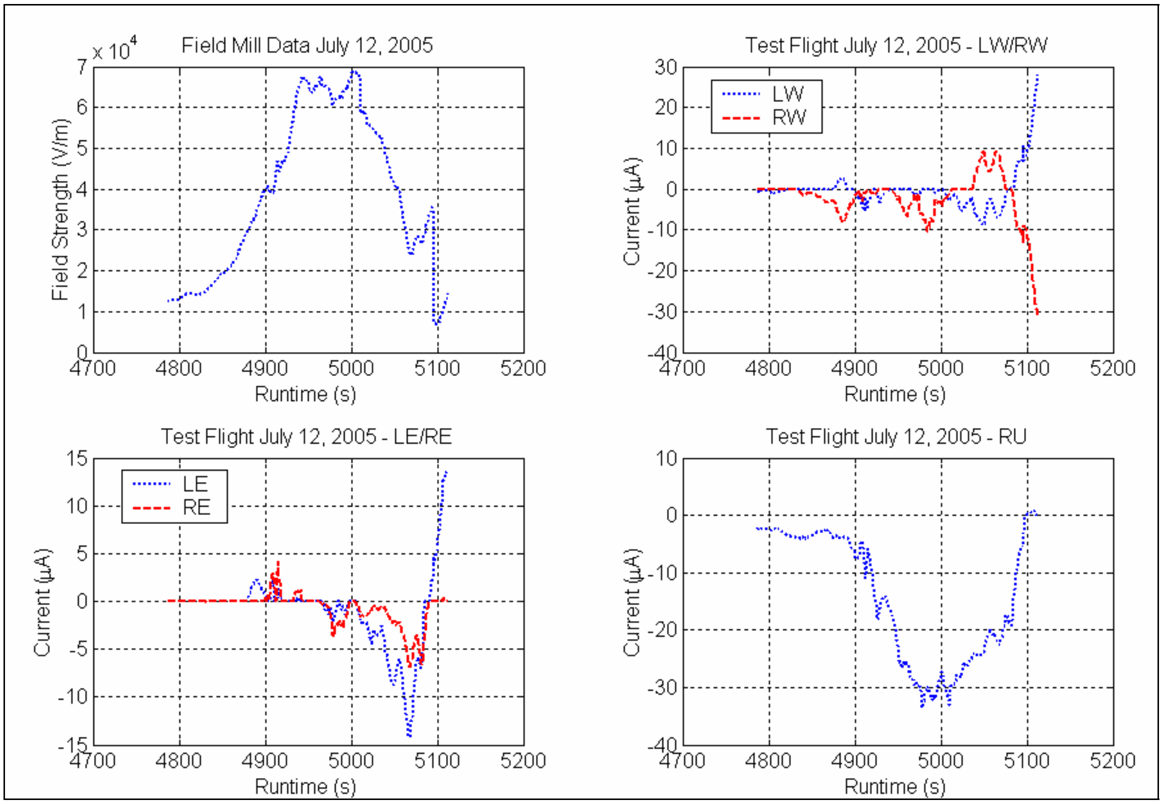

Figure C5: Data Charging System Results

Appendix D

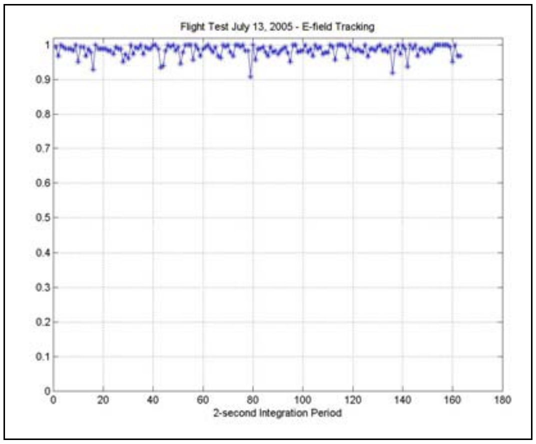

Figure D1: E-field Tracking Results

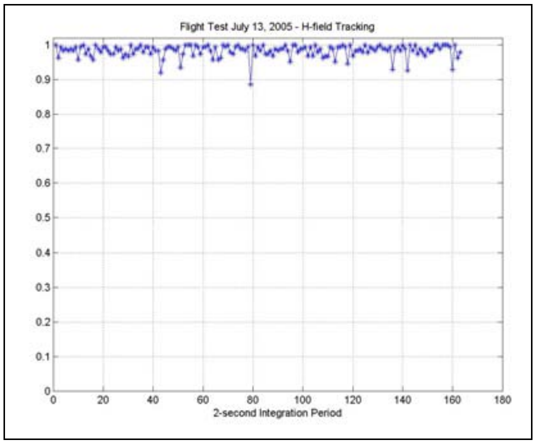

Figure D2: H-field Tracking Results

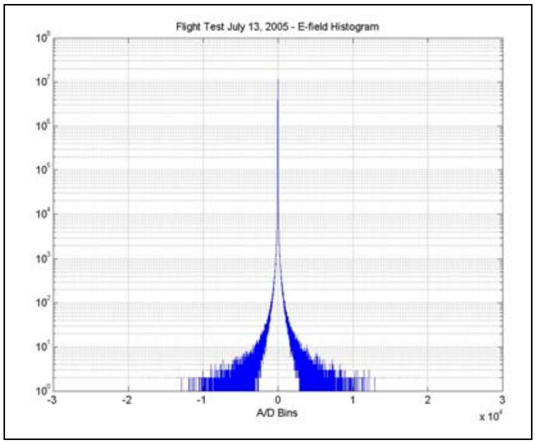

Figure D3: E-field Histogram

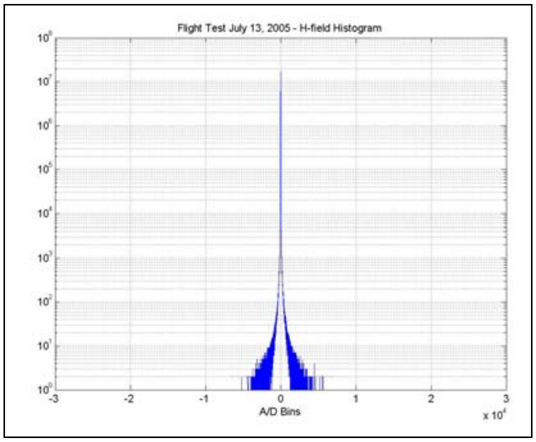

Figure D4: H-field Histogram

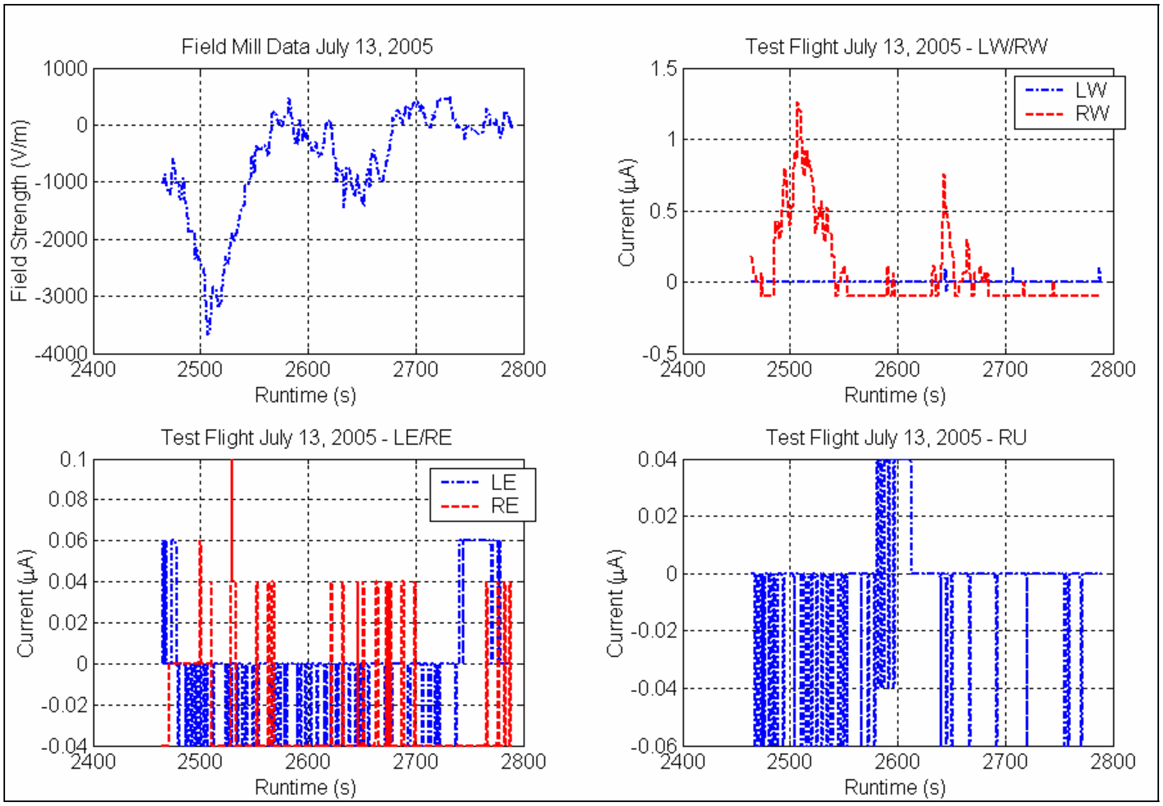

Figure D5: Data Charging System Results